Adsorption (2006) 12:19–26
DOI 10.1007/s10450-006-0135-2

Use of x-ray microtomography to visualise dynamic adsorption of organic vapour and water vapour on activated carbon

P. Lodewyckx · S. Blacher · A. Léonard

Received: 21 February 2006 / Revised: 15 May 2006 / Accepted: 7 July 2006

Abstract X-ray microtomography coupled with image analysis was used to quantify the adsorption of vapours on activated carbon beds. This technique was tested using three different challenges: CCl_4, water vapour and a mixture of water- and organic vapour. It is shown that the used technique allows determining the adsorption front progress in the case of organic vapour and mixture of water and organic vapour whereas the existence of this front was not so obvious in the case of water vapour. Experimental results obtained for organic vapours were interpreted on the basis of the Wheeler-Jonas equation: a good agreement was found between experimental and theoretical breakthrough times.

Keywords Activated carbon · Adsorption · Tomography · Modelling

1 Introduction

The better knowledge of vapour adsorption dynamics is of high importance for both civil and military protection. When modelling organic vapour adsorption on activated carbon beds, one has to take into account the effects of water-vapour co-adsorption (Lodewyckx and Vansant, 1999, 2000). Both the pre-adsorbed water and the water present in the contaminated air stream can have a deleterious effect on the adsorption capacity of the activated carbon. This explains the renewed interest in the adsorption behaviour of water vapour on activated carbon. A good overview of recent publications in this area can be found in Brennan et al. (2001). However, this attention has been, almost exclusively, focussed on the static adsorption capacity, *i.e.* the water vapour adsorption isotherm. Even though this static capacity is very important, adsorption (and especially co-adsorption) is essentially a dynamic phenomenon. Apparently, there is no exploitable model available for the kinetics of water adsorption. The existing ones are semi-empirical, usually based on a linear driving force model (Foley et al., 1997; Lodewyckx and Vansant, 1998).

The first purpose of this work is to assess the suitability of x-ray microtomography to follow adsorption phenomena taking place in activated carbon beds. The very first use of X-ray imaging, in radiography mode, to study adsorption in porous materials was performed by Dubinin et al. (1975). In this pioneer work, they employed X-ray contrast substances to analyse the nature of the mass transfer limiting step, *i.e.* adsorption in micropores or transport in meso and macropores, in activated carbons. Gravimetric measures were used to determine separately the diffusion coefficients of

P. Lodewyckx (✉)
Royal Military Academy, Department of Chemistry, Renaissancelaan 30, B-1000 Brussels, Belgium

S. Blacher · A. Léonard
University of Liège – Dept. Applied Chemistry, Lab. Chemical Engineering – Sart-Tilman B6, B-4000 Liège, Belgium
e-mail: a.leonard@ulg.ac.be

Table 1 Experimental conditions for the H_2O, CCl_4 and $CCl_4 + H_2O$ dynamic adsorption experiments.

Vapour	Concentration	Breakthrough criterion
H_2O	80% RH	not determined
CCl_4	5 g/m^3	50 mg/m^3
CCl_4	5 g/m^3	50 mg/m^3
$+ H_2O$	80% RH	not determined
Test conditions:	Volumetric flow rate = 10000 cm^3/min	
	Filter diameter = 15 mm	
	Total filter depth = 25 mm	
	Investigated filter depth = 20 mm	
	Test temperature = 293 K	
	Carbon type = BPL	
	Carbon mass = 1.6 g	

both transfer mechanisms. X-ray radiographies served as visual supports to explain adsorption kinetics data but no quantification was performed. The X-ray technique was taken up only 15 years after by Wittwer and Lavanchy (1990), to visualise, in a medical tomograph, the adsorption of organic vapours in activated carbon. To our knowledge, this non-destructive 3D-technique has not been exploited much since the early 90's. During the last decade, the development of microfocus X-ray sources and high resolution CCD detectors led to the commercialisation of microtomographs with improved resolution and large field of applications. The objective of the present study is to contribute to a better understanding of the dynamics of water vapour adsorption by leaning on the local information obtained by x-ray microtomography coupled with image analysis. Though there exist other imaging techniques like magnetic resonance imaging (Bar et al., 2000) or positron emission profiling (Schumacher et al., 2000) providing a much larger wealth of information, they are much more expensive and not as easily accessible as x-ray microtomography.

2 Experimental

2.1 Adsorption set-up

A plastic, cylindrical canister (diameter = 15 mm and height = 25 mm) filled with 1.6 g of BPL activated carbon was used to perform the adsorption tests in a classical breakthrough measurement system. Due to the space limitations in the tomograph, the height and, especially, the diameter of the bed had to be severely reduced compared to filters commonly used. Experiments were conducted successively for CCl_4 in dry air, CCl_4 in humid air (= water-organic co-adsorption), and humid air at the same temperature and flow rate, as indicated in Table 1. For each test, one out of the three gases was forced through the bed with renewed carbon during 3, 6 and 9 minutes. Tomographic investigations of the beds were performed before and after exposure to the vapours.

2.2 X-ray microtomograph

X-ray microtomography is a powerful non-invasive technique allowing the visualization of the internal texture of a sample based upon local variation of the x-ray attenuation coefficient. It was used to obtain 2-dimensional cross sections images of the carbon bed. During tomographic investigation, an X-ray beam is sent on the sample and the transmitted beam is recorded with a detector. According to the Beer-Lambert law, the transmitted intensity is related to the integral of the X-ray attenuation coefficient along the path of the beam, μ. This coefficient μ depends on the material density, ρ, the atomic number of the material, Z, and on the energy of the incident beam, E, according to Eq (1):

$$\mu = \rho\left(\mathrm{a} + \frac{\mathrm{b}Z^{3.8}}{E^{3.2}}\right) \tag{1}$$

where a and b are energy-dependent coefficients (Vinegar and Wellington, 1987). Projections (defined by the assembling of transmitted beams) are recorded for several angular positions by rotating the sample between 0 and 180°. Then a back-projection algorithm is used to reconstruct 2D or 3D images, depending on the method used. In the case of 2D images, each pixel is characterized by a grey level value corresponding to the local attenuation coefficient.

The x-ray tomographic device used in this study was a "Skyscan-1074 X-ray scanner" (Skyscan, Belgium).

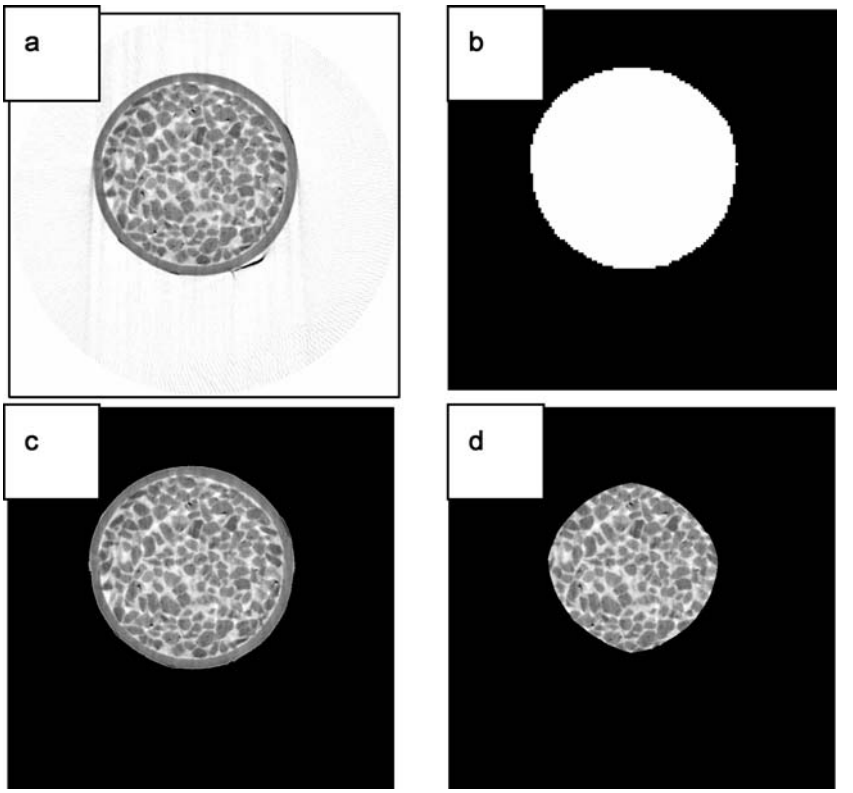

Fig. 1 Image analysis processing – a. original cross section image b. binary mask c. elimination of background d. erosion of the image to exclude border effects

Advanced technical details about its conception and operation are described by Sasov and Van Dyck (1998). The cone beam source operated at 40 kV and 1 mA. The detector was a 2D, 768 pixels $\times$ 576 pixels, 8-bit X-ray camera with a spatial resolution of 41 μm. The rotation step was fixed at the minimum, 0.9°, in order to improve image quality, giving total acquisition times close to 8 minutes. For each angular position a radiograph of the whole bed, instead of a 1D-projection of a cross section, was recorded by the 2D camera. In contrast to a classical medical scanner, the source and the detector were fixed, while the sample was rotated during the measurement. Once the sample was placed into the microtomograph, the scanning was performed, allowing the investigation of a height of max 25 mm. Cross sections separated by 205 μm were reconstructed along the carbon bed using a cone beam reconstruction software. However, the tomographic images of the bottom part of the filter were cluttered by the construction of the filter. For this reason only the first 20 mm of the filter were used for quantification.

2.3 Image analysis

Image analysis was performed using the Aphelion3.2 (Adsis) software on a PC that allowed implementing algorithms using signal processing and tools from mathematical morphology (Soille, 1999). The developed image analysis algorithm was based on the observation that the grey level intensity of the carbon grains darkens when vapour is adsorbed. Taking this into account, image analysis was performed on each cross section according to the following steps: from original grey-level image cross-section (Fig. 1(a)), a binary mask was automatically constructed (Fig.1(b)) and used in order to isolate the bed from the background (Fig. 1(c)). Next, the image was eroded to eliminate possible borders effects (Fig. 1(d)). On this last image, the intensity, *i.e.* the addition of all the pixel values of the grey level image, was calculated. The intensity of the approximately 100 cross-sections images per sample was determined and the result drawn in function of the depth of the sample, *i.e.* the distance from the inlet of the carbon bed.

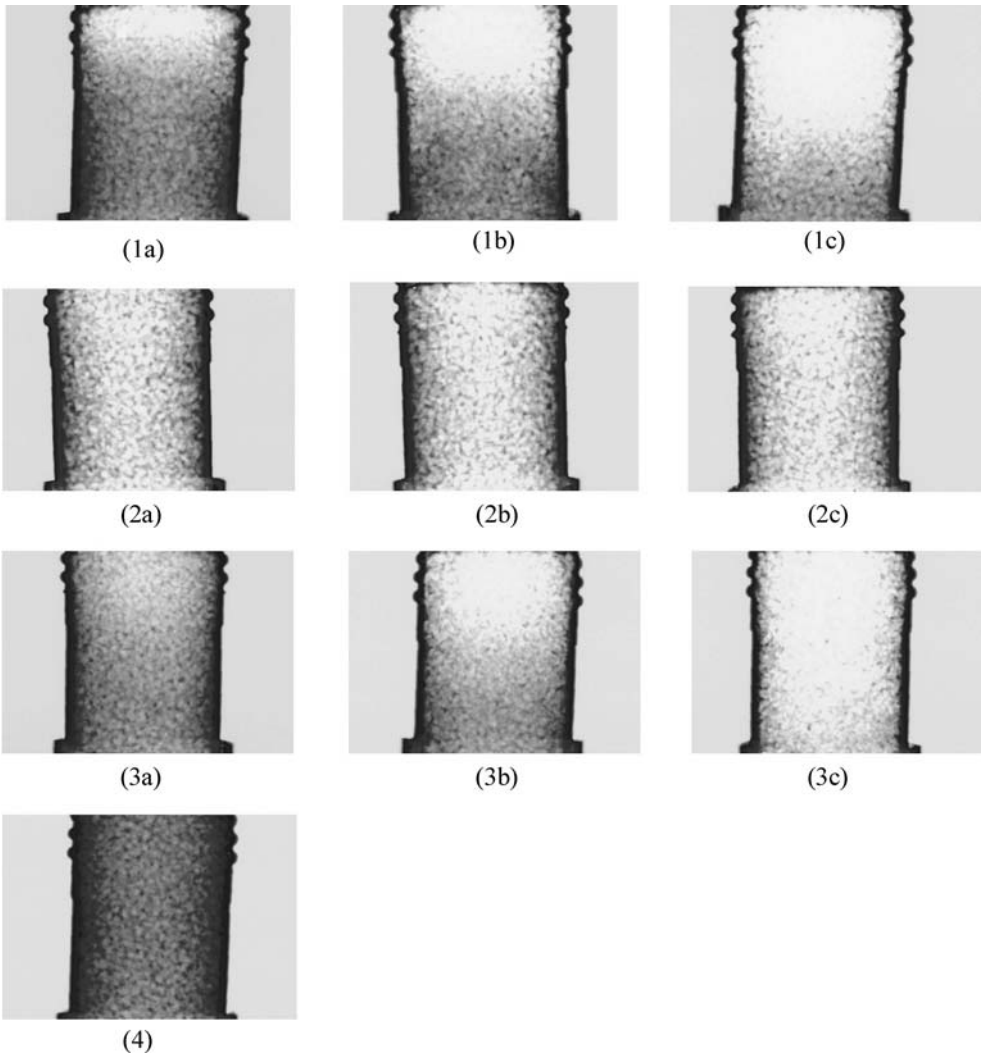

Fig. 2 Radiographs of the carbon bed during adsorption of CCl_4 (1), H_2O (2) and $CCl_4 + H_2O$ (3). Respectively after 3 (a), 6 (b) and 9 minutes (c). Comparison with "virgin" (initial) carbon bed (4)

3 Results and discussion

3.1 Qualitative results: radiographs observation

Radiographs of the carbon bed in which different gases were adsorbed are shown in Fig. 2. From these images two features can be observed: for one, variations of the grey level intensity which represent the adsorption progress and the adsorption front in the case of CCl_4, are clearly visible. Secondly, the evolutions of the grey level intensities for CCl_4, water and water-organic vapour adsorption, are visibly not the same which suggests different adsorption mechanisms. To quantify these two qualitative observations, the grey level intensity of successive cross section tomographic images as a function of filter depth was determined, according to the image analysis processing previously described. The intensity (y-axis) in Figs. 3.4 and 5 is given in arbitrary units as only the relative difference between the intensity of images at different time intervals is relevant for our study.

3.2 CCl_4 adsorption

The CCl_4 adsorption as a function of time is visualised in Fig. 3. The adsorption proceeds according to the theoretical model of a plug flow, *i.e.* one can see an adsorption front that moves through the carbon bed. Upstream

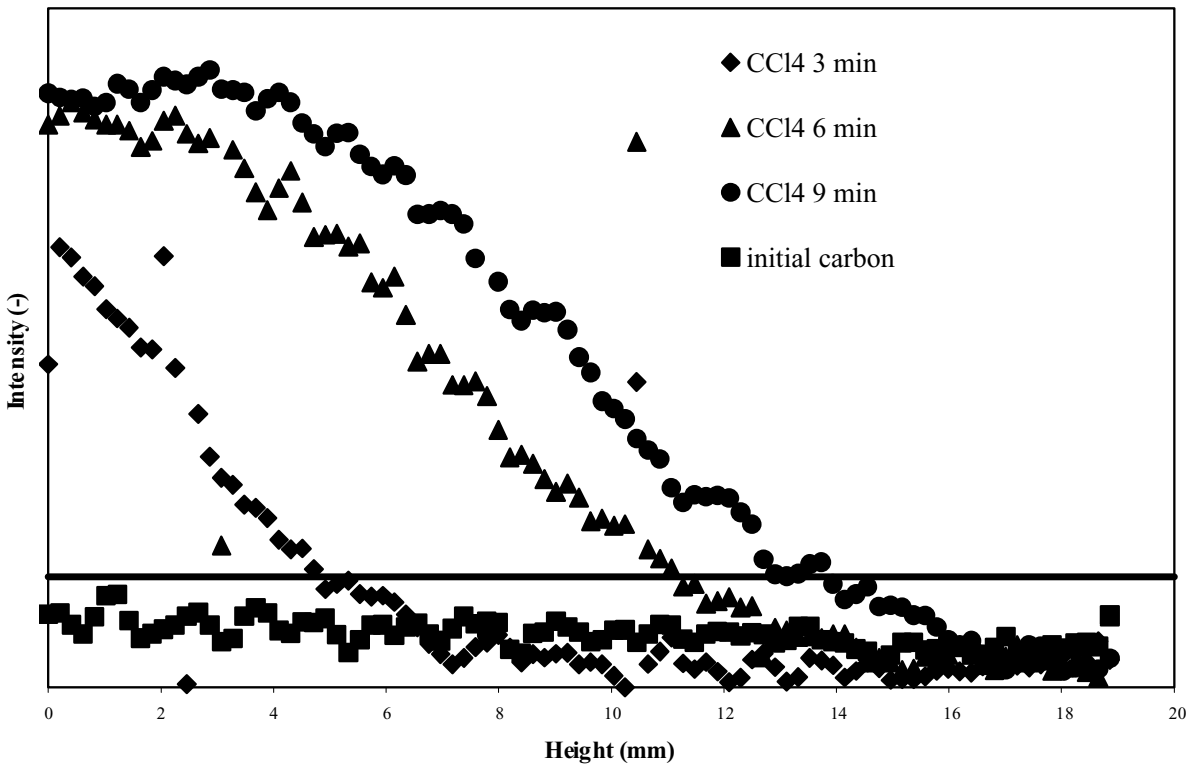

Fig. 3 Intensity (arbitrary units) versus bed depth for different exposure times to pure CCl_4 in dry air

of this front there is saturation of the carbon (clearly visible after 9 minutes), downstream the carbon is still in its initial state. The existence of a single, constant, front is further proven by the fact that the concentration profiles after 3, 6 and 9 minutes are clearly parallel.

During the experiment the exit concentration of CCl_4 was monitored with an IR-spectrometer Miran 1B2 (Foxboro). Usually the breakthrough criterion for this kind of tests is taken at 0.1 to 1% of the inlet concentration. However, on the tomographic images it is impossible to distinguish this small amount of CCl_4, as it disappears into the clutter of the baseline (*i.e.* the carbon before adsorption). Therefore the breakthrough criterion was set at 10%. This is visualised in Fig. 3 by the horizontal line at 10% between the baseline and the mean value of the saturation part at 9 minutes. With this criterion**,** breakthrough of the bed was detected after 12 minutes. This was further verified by modelling the adsorption with the Wheeler-Jonas equation (Eq 2) (Jonas and Rehrmann, 1973) and the annex equations proposed by Wood (1992) and Lodewyckx-Wood (2003).

$$t_b = \frac{W_e\, M}{c_{\text{in}}\, Q} - \frac{W_e \rho_b}{k_v c_{\text{in}}} \ln\left[\frac{c_{\text{in}} - c_{\text{out}}}{c_{\text{out}}}\right] \tag{2}$$

These equations have been adequately verified and the resulting breakthrough times are very reliable (less than 10% error margin). As the last picture was taken after 9 minutes, it is impossible to verify the breakthrough time by tomography. Therefore the calculations were repeated for an imaginary filter of 1 cm bed depth. Here the theoretical calculation gives a breakthrough after 6 minutes (rounded up). This is in agreement with Fig. 3: it is clear that the front passes the intersection of the 10% line with the 10 mm mark a few seconds before 6 minutes. This means there is a very good agreement between the theoretical and experimental breakthrough times and the tomographic images.

3.3 Water adsorption

The situation is quite different in the case of pure water vapour adsorption (see Fig. 4). The scatter on the data is extremely high. This was already visible on the image

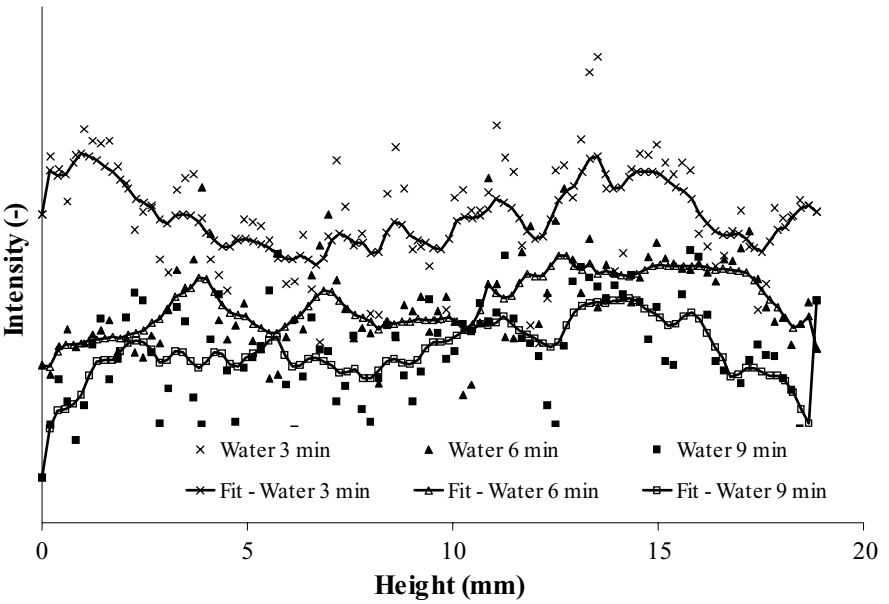

Fig. 4 Intensity (arbitrary units) versus bed depth for different exposure times to pure water vapour (80% RH) in air

itself (Fig. 2), where the difference between 3, 6 and 9 minutes is hardly noticeable and there is no visible adsorption front (comparing *e.g.* Fig. 1(b) with 2(b)).

In order to extract some information, for each exposure time, a smooth curve was fitted for each point using locally weighted (10% of data) least-squares (Stineman, 1980) (see Fig. 4). This kind of curve fit allowed distinguishing if some trend in the adsorption front evolution existed. The obtained smooth curves suggest that: apparently, water vapour adsorption does not show an adsorption front moving through the filter. Instead, the whole bed becomes more and more saturated with adsorbed water. These results are in agreement with previous experiments (Lodewyckx et al., 2005) and breakthrough data (Cosnier et al., 2005). In terms of the plug flow model, described by the Wheeler-Jonas equation, this can be interpreted as a very slow adsorption process, *i.e.* an extremely low value of the overall mass transfer coefficient k_v in equation 1. In the earlier X-ray experiments performed by Dubinin et al. (1975), this was attributed to the diffusion resistance in the adsorption pores, *i.e.* the micropore system, being much higher than the resistance in the transport pores (macro- and mesopore system). However, they did not provide any explanation for this event. Possibly it is the same phenomenon as for organic vapours for which they demonstrated a clear positive relation between inlet concentration and diffusion control by resistance in the adsorption pores. In the present work, water adsorption experiments being carried out by 80%RH (See Table 1) it is safe to say water vapour inlet concentration was very high. Hence the experimental observation of water adsorption kinetics being apparently determined by micropore resistance (surface diffusion) could be a direct effect of this high inlet concentration.

3.4 Water-organic vapour co-adsorption

The results of water-organic vapour co-adsorption are represented in Fig. 5. The image is very clear, and the adsorption front is visible. The interpretation however is not straightforward: the density change is due to both adsorbed organic vapour and water, and it is difficult to make a distinction between both phases. This is confirmed by comparing Fig. 5 with the experimental and calculated breakthrough times. For the latter we used an adapted version of the Wheeler-Jonas equation in order to include the effects of water vapour co-adsorption. In this model the capacity (W_e) and kinetic (k_v) parameters of Eq. 2 are not considered to be constants. They depend on the amounts of water present on the carbon and in the air stream as these will compete with the organic vapour for available adsorption space (Lodewyckx and Vansant, 1999, 2000). The tomographic image shows a "breakthrough" between 3 and 6 minutes. Experimentally, the breakthrough of CCl_4 under these conditions of relative humidity was detected after 8 minutes. The same result was obtained by the simulation. Clearly,

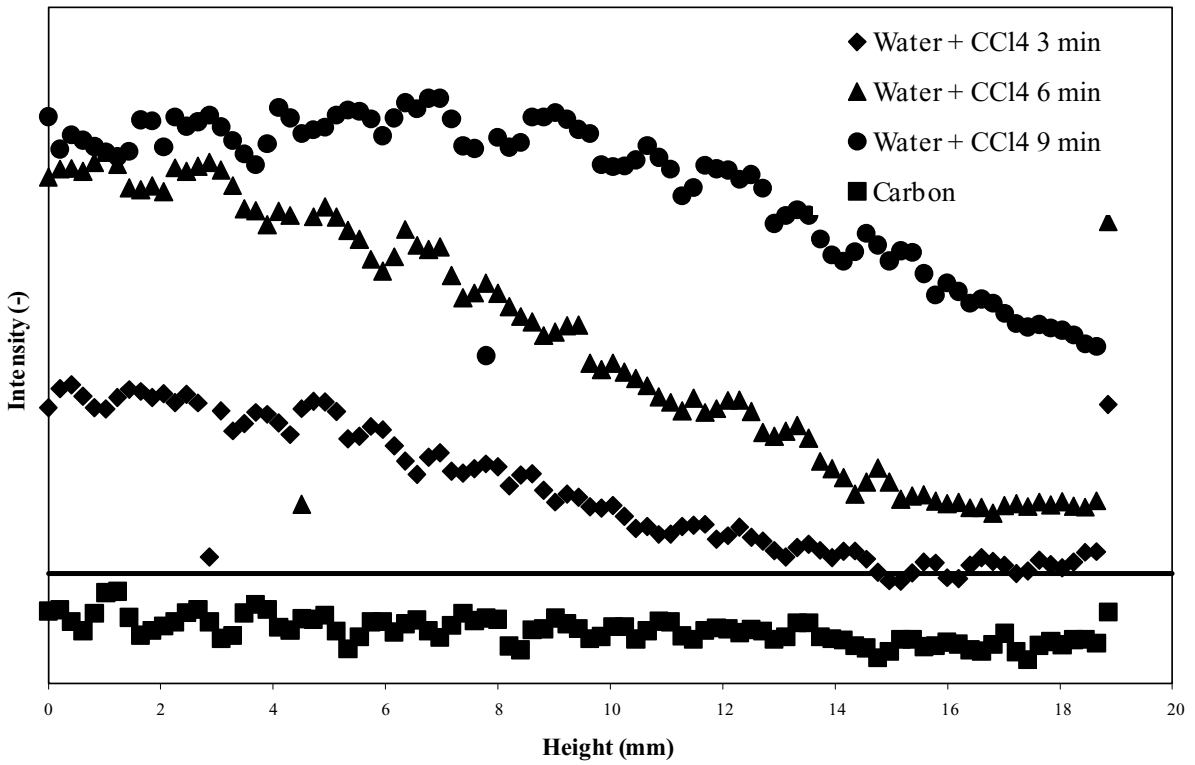

Fig. 5 Intensity (arbitrary units) versus bed depth for different exposure times to CCl_4 in air with a RH of 80%

there is a difference of 50 to 100% with the breakthrough of the front obtained from the tomographic images. Hence we can conclude that this front, although apparently a CCl_4 front (comparing Figs. 5, 4 and 3) is in fact a mixed front. This could also explain its broadness: the front is clearly broader than in the case of pure CCl_4, even though it is still visible, thus steeper than in the case of pure water vapour. Another interesting feature is the fact the front remains roughly constant: as it is the case for pure CCl_4, the concentration profiles after 3, 6 and 9 minutes are almost parallel, even though their slope it quite different from the one in Fig. 3.

4 Conclusions

The results presented in this work show that x-ray microtomography coupled with image analysis constitutes a very promising technique to visualise and quantify the adsorption of vapours on activated carbon. Especially in the case of organic vapours, such as CCl_4, one gets a clear image of the macroscopic adsorption process. It is however difficult to use this technique to determine breakthrough of the bed, especially at low concentration.

In the case of water vapour adsorption, the observations seem to indicate another type of phenomenon with progressive water uptake through the bed: this apparent dependence of water vapour adsorption kinetics on micropore resistance needs further investigation. The water vapour adsorption images are however consistent with previous experiments and breakthrough data. Some of the differences could also result from the limited sensitivity of the used tomograph versus adsorbed water. Indeed, a better contrast is obtained with organic vapours characterized by higher densities than water.

One possible way to confirm these results is the use of an x-ray microtomograph with higher resolution (down to 5 μm) and extended possibilities in term of X-ray energy selection, in order to improve image quality and to get a better discrimination between the phases, *i.e.* water, organic and carbon, by applying a more sophisticated image analysis procedure. This will also be helpful for the interpretation of co-adsorption images, which remains difficult for the time being, in order to correlate with breakthrough data. Another

possibility consists in increasing the number of images (*e.g.* every minute in stead of every three minutes) and the amount of carbon in order to obtain more information that can show general trends. It will also be very interesting to perform a tomographic investigation very shortly after the start of the experiment: breakthrough curve analysis (Cosnier et al., 2005) has shown the presence of an adsorption front for water adsorption, but only at the very start of the experiment. After this initial phase all known experiments show the adsorption behaviour that is exhibited in Fig. 4.

Nomenclature

μ = x-ray linear attenuation coefficient, 1/m
ρ = bulk density, kg/m^3
ρ_b = bulk density of the carbon bed, g_{carbon}/cm^3
a = energy-dependent coefficient, [-]
b = energy-dependent coefficient, [-]
c_{in} = contaminant concentration in air, g/cm^3
c_{out} = chosen breakthrough concentration, g/cm^3
k_v = overall adsorption rate coefficient, 1/min
E = X-ray energy, kV
M = weight of the carbon bed, g_{carbon}
Q = volumetric flow rate, cm^3/min
t_b = breakthrough time to reach c_{out} , min
W_e = equilibrium adsorption capacity, g/g_{carbon}
Z = atomic number, [-]

Acknowledgements The authors wish to thank the technicians of the Belgian Defence Laboratories (DLD), for their much appreciated help with the experimental part of this work, as well as CHEMVIRON (Belgium) for kindly providing the carbon samples.

A. Léonard is indebted to the Belgian Fonds National de la Recherche Scientifique (FNRS) for a position of Postdoctoral Researcher.

S. Blacher acknowledges the ALFA Program of the E.U. (project ALFA II 0412 FA FI) for enabling fruitful exchanges.

References

Bar, N.-K. and B.J.R.D.M. Balcom, "Direct Measurement of Transient Concentration Profiles in Molecular Sieve Particles and Columns by MRI," *Adsorption Science and Technology*, D.D. Do (ed), pp. 6–13, World Scientific, Singapore, 2000.

Brennan, J.K., T.J. Bandosz, K.T. Thomson, and K.E. Gubbins, "Water in porous carbons," *Colloid Surface A*, **187–188**, 539–568 (2001).

Cosnier, F., A. Celzard, G. Furdin, D. Bégin, and J.F. Marêché, "Influence of water on the dynamic adsorption of chlorinated VOCs on activated carbon: relative humidity of the gas phase versus pre-adsorbed water," *Proceedings of Carbon 2005, Gyeongju, Korea, July 3–7*, 2005.

Dubinin, M.M., I.T. Erashko, O. Kadlec, V.I. Ulin, A.M. Voloshchuk, and P.P. Zolotarev, "Kinetics of physical adsorption by carbonaceous adsorbents of biporous structure," *Carbon*, **13**, 193–200 (1975).

Foley, N.J., K.M. Thomas, P.L. Forshaw, D. Stanton, and P.R. Norman, "Kinetics of Water Vapor Adsorption on Activated Carbon," *Langmuir*, **13**, 2083–2089 (1997).

Jonas, L.A. and J.A. Rehrmann, "Predictive equations in gas adsorption kinetics," *Carbon*, **11**, 59–64 (1973).

Lodewyckx, P., A. Léonard, and S. Blacher, "The use of tomography to determine the kinetics of water vapour adsorption," *Proceedings of Carbon 2005, Gyeongju, Korea, July 3–7, 2005* (2005).

Lodewyckx, P. and E.F. Vansant, "The dynamic adsorption of water vapour on activated carbon," *Carbon*, **36**, 304 (1998).

Lodewyckx, P. and E.F. Vansant, "Influence of humidity on adsorption capacity from the Wheeler-Jonas model for prediction of breakthrough times of water immiscible organic vapors on activated carbon beds," *AIHA J.*, **60**, 612–617 (1999).

Lodewyckx, P. and E.F. Vansant, "The influence of humidity on the overall mass transfer coefficient of the Wheeler-Jonas equation," *AIHA J.*, **61**, 461–468 (2000).

Sasov, A. and D. Van Dyck, "Desktop X-ray microscopy and microtomography," *J. Microsc.*, **191**, 151–158 (1998).

Schumacher, R.R., B.G. Anderson, N.J. Noordhoek, F.J.M.M. de Gauw, A.M. de Jong, M.J.A. de Voigt, and R.A. van Santen, "Tracer-exchange experiments with positron emission profiling: diffusion in zeolites," *Microporous and Mesoporous Materials*, **35–36**, 315–326 (2000).

Soille, P., *Morphological Image Analysis – Principles and Applications*, Springer-Verlag, New York (1999).

Stineman, R.W., "A consistently well-behaved method of interpolation," *Creative Comput.*, **6**, 54–57 (1980).

Vinegar, H.J. and S.L. Wellington, "Tomographic imaging of three-phase flow experiments," *Rev. Sci. Instrum.*, **58**, 96–107 (1987).

Wittwer, A. and A. Lavanchy, "X-ray computer tomography: A non destructive method to investigate dynamic sorption processes on activated carbon," *Proceedings of the International Carbon Conference, Paris, France, 1990,* 102–103 (1990).

Wood, G.O., "Activated carbon adsorption capacities for vapors," *Carbon*, **30**, 593–599 (1992).

Wood, G.O. and P. Lodewyckx, "An extended equation for rate coefficients for adsorption of organic vapors and gases on activated carbons in air-purifying respirator cartridges," *AIHA Journal: a Journal For The Science Of Occupational And Environmental Health And Safety*, **64**, 646–650 (2003).